Centroid motion in periodically focused beams

J. S. Moraes, R. Pakter, and F. B. Rizzato

Citation: Physics of Plasmas **12**, 023104 (2005); doi: 10.1063/1.1848546
View online: http://dx.doi.org/10.1063/1.1848546
View Table of Contents: http://scitation.aip.org/content/aip/journal/pop/12/2?ver=pdfcov
Published by the AIP Publishing

Centroid motion in periodically focused beams

J. S. Moraes[a)]
Centro Universitário La Salle, Avenida Victor Barreto, 2288, 92010-000 Canoas, RS, Brazil and Instituto de Física, Universidade Federal do Rio Grande do Sul, Caixa Postal 15051, 91501-970 Porto Alegre, Rio Grande do Sul, Brazil

R. Pakter[b)] and F. B. Rizzato[c)]
Instituto de Física, Universidade Federal do Rio Grande do Sul, Caixa Postal 15051, 91501-970 Porto Alegre, Rio Grande do Sul, Brazil

(Received 6 July 2004; accepted 23 November 2004; published online 12 January 2005)

The role of the centroid dynamics in the transport of periodically focused particle beams is investigated. A Kapchinskij–Vladimirskij equilibrium distribution for an off-axis beam is derived. It is shown that centroid and envelope dynamics are uncoupled and that unstable regions for the centroid dynamics overlap with previously stable regions for the envelope dynamics alone. Multiparticle simulations validate the findings. The effects of a conducting pipe encapsulating the beam are also investigated. It is shown that the charge induced at the pipe may generate chaotic orbits which can be detrimental to the adequate functioning of the transport mechanism. © *2005 American Institute of Physics*. [DOI: 10.1063/1.1848546]

I. INTRODUCTION

A common practice in the analysis of intense beam transport in confining systems with periodical focusing is to take the beam centroid as perfectly aligned with the system axis.[1–5] This is often a suitable assumption as the axis is an equilibrium for the centroid. This equilibrium is even predominantly stable if smooth-beam approximations are employed where periodic fluctuatons of the focusing lattice is averaged out.[6] Parametric resonances involving the centroid motion and the lattice can, however, affect stability when the oscillatory frequency of the centroid and the lattice periodicity are commensurable, which prohibits averaging techniques. This sort of instability adds some operational restrictions to those already resulting from requirements on stability of beam envelope dynamics, if stable regions for the envelope dynamics overlap with unstable regions for the centroid dynamics.

Pure envelope dynamics has been the subject of recent studies searching for stable operational regions in a parametric plane defined by the focusing field profile and intensity, which are relevant control parameters for this sort of system.[7] Drawing attention to solutions with the same periodicity as the focusing lattice—we call these solutions *matched solutions*—previous results point to the fact that stable regions exist and are separated from each other by a series of openings where the matched solutions are either unstable or simply do not exist.[8–10] Unstable regions of envelope dynamics are immediately discarded from the set of operational regions for beam transport, so we are interested in how the *stable* envelope regions respond to the centroid dynamics. Destabilization due to centroid should be viewed as a further restriction, reducing the available operational parameter space.

The idea here is therefore to perform an analysis of the combined centroid and envelope motion under the influence of a periodic focusing lattice. We first consider vacuum propagation of a homogeneous density beam in solenoidal focusing structure neglecting wall effects, since this model is sufficiently generic to represent what happens in a variety of similar situations.[4,11] It is demonstrated that a Kapchinskij–Vladimirskij (KV) equilibrium distribution exists for off-axis beams, and the equations for the evolution of the centroid and the envelope are derived accordingly. We show that regions of unstable centroid dynamics can indeed overlap with stable regions for the envelope dynamics alone, and that this overlap is persistent as the profile of the focusing lattice is varied from sinusoidal to sharp-edged shapes. As mentioned, this instability results from the beating of lattice and centroid periodicites; it does not exist in homogeneous systems but must be treated with care in periodic schemes of confinement. The analysis is supplemented with simulations involving a large number of macroparticles, which show that the low-dimensional approach based on envelope and centroid equations is quite precise.

On grounds of Gauss' law and symmetry considerations one concludes that influence of conducting pipes on the envelope dynamics is null in axisymmetric geometries with exactly on-axis beams.[12] Even in more complex and general geometries, like those based on alternating gradient quadrupoles, influence is found to be weak.[13] Influence of pipes on the centroid dynamics has been studied as well, but only under smooth-beam approximations as mentioned earlier.[6] It is therefore appropriate to look at this latter issue when smooth-beam approximations fail, and we develop the pertinent analysis in the last part of this paper. We show that the centroid dynamics may become chaotic as the nonlinear effects of the conducting walls are included. The chaotic region does not extend down to the axis, but under some con-

[a)]Electronic mail: jsmoraes@if.ufrgs.br
[b)]Electronic mail: pakter@if.ufrgs.br
[c)]Electronic mail: rizzato@if.ufrgs.br

ditions can get very close to it threatening the nonlinear stability of the transport scheme.

The paper is organized as follows. In Sec. II we define the model and introduce the methods of analysis to be employed. In Sec. III we map various stable and unstable regions both for the centroid and envelope motion, with help of root finder algorithms and full multiparticle simulations. Finally in Sec. IV we summarize the work.

II. MODEL AND METHODS

Consider an intense continuous beam transported with constant axial velocity in a periodically focusing magnetic channel in the absence of boundaries. When the beam is perfectly aligned with the transport axis, which we take as the z axis, the appropriate equation describing the envelope r_b reads

$$r_b''(s) + \kappa_z(s) r_b = F(r_b), \tag{1}$$

where we introduce the common notation $s \equiv z$ of physics of beams, the primes denoting derivatives with respect to s. The focusing field is characterized by the focusing strength parameter $\kappa_z(s+S) = \kappa_z(s)$, where S is the periodicity length of the channel. κ_z is related to the magnetic field $B_z(s)$ by $\kappa_z(s) = q^2 B_z^2(s)/4\gamma_b^2\beta_b^2 m^2 c^4$, where q, m, and $\gamma_b = (1-\beta_b^2)^{-1/2}$ are, respectively, the charge, mass, and relativistic factor of the beam particles. The average κ_z over one period of the lattice is designed in the form $\overline{\kappa_z(s)} \equiv (1/S)\int_0^S \kappa_z(s)ds \equiv \sigma_0^2/S^2$; σ_0 is proportional to the rms focusing field and measures the vacuum phase advance in the small field, smooth-beam approximation. The "force" $F(r_b)$ reads $F(r_b) = \epsilon^2/r_b^3 + K/r_b$, where $K = 2q^2 N_b/\gamma_b^3\beta_b^2 mc^2$ is the beam perveance, ϵ is the unnormalized emittance of the beam, and N_b is the number of particles per unit axial length. All information about the focusing field is contained in $\kappa_z(s)$. In particular, we show in Ref. 7 that a wide range of field profiles can be adequately modeled by a suitable parametrization of κ_z in the form

$$\kappa_z(s) = \frac{\sigma_0^2}{S^2}\left[\frac{1+\cos\theta(s)}{\mathcal{N}}\right], \tag{2}$$

with the phase function given by

$$\theta(s) = \pi\left\{\frac{\tan^{-1}[\Delta(\bar{s}+\eta/2)] + \tan^{-1}[\Delta(\bar{s}-\eta/2)]}{\tan^{-1}[\Delta(1+\eta)/2] + \tan^{-1}[\Delta(1-\eta)/2]}\right\}. \tag{3}$$

$\mathcal{N} = 1 + (1/S)\int_0^S \cos\theta(s)ds$ is used as a normalization factor, $\bar{s} = \mathrm{mod}(s/S + 1/2, 1) - 1/2$ is periodic in s and always lies in the range $-1/2 \geqslant \bar{s} \geqslant 1/2$, $\Delta > 0$ is the focusing field profile parameter, and $0 < \eta \leqslant 1$ is the filling factor. Function $\kappa_z(s)$ in Eq. (2) is constructed such that for small Δ it resembles a smooth sinusoidal function of period 1 in s, while for larger Δ's it develops sharper edges, eventually turning into a discontinuous periodic step function. In fact, one shows that when $\Delta \ll 1$

$$\kappa_z(s) = \frac{\sigma_0^2}{S^2}\left[1 + \cos\left(\frac{2\pi}{S}s\right)\right], \tag{4}$$

and that when $\Delta \gg 1$

$$\kappa_z(s) = \begin{cases} 0, & \eta/2 < s/S < 1 - \eta/2 \\ \dfrac{\sigma_0^2}{\eta S^2}, & \text{otherwise.} \end{cases} \tag{5}$$

Note that for all Δ, the denominator in Eq. (3) guarantees that the phase function completes a full cycle from $\theta = -\pi$ to $\theta = \pi$ as $\bar{s}$ goes from $-1/2$ to $1/2$, and consequently $\kappa_z(s)$ is always continuous at the lattice boundaries.

Now we proceed to show that even when the beam is not perfectly aligned with the axis, Eq. (1) still describes the beam envelope, the difference with respect to previous analyses being an additional equation governing the centroid. This results in part from the fact that the focusing term is linear in the coordinates as we shall see now. Consider the beam as formed by a group of macroparticle charged rods. Each rod follows an equation of the form

$$\mathbf{r}'' = -\kappa_z(s)\mathbf{r} - \boldsymbol{\nabla}_\perp \psi(\mathbf{r}, s) \tag{6}$$

in the rotating Larmor frame.[2,4] $\mathbf{r} = \mathbf{r}(s) = [x(s), y(s)]$, $\perp$ selects the transverse component of the gradient, and ψ denotes the normalized electromagnetic potential felt by the macroparticle under analysis. It is related to the electrostatic potential ϕ through $\psi = q\phi/\gamma_b^3 m\beta_b^2 c^2$ and satisfies the Poisson equation

$$\nabla_\perp^2 \psi = -(2\pi K/N_b) n(x, y, s). \tag{7}$$

$n(x, y, x)$ denotes the transversal particle density obtained in the form $n = \int f dx' dy'$, and $f = f(\mathbf{r}, \mathbf{r}', s)$ is the particle distribution function that must satisfy the stationary Vlasov equation $df/ds = 0$.[2,4] Summing Eq. (6) over all beam particles (rods) and dividing by their total number N_b one arrives at

$$\mathbf{r}_o'' = -\kappa_z(s)\mathbf{r}_o, \tag{8}$$

where $\mathbf{r}_o \equiv 1/N_b \Sigma_{j=1}^{N_b} \mathbf{r}_j$ is the averaged or beam centroid coordinate, and $\Sigma_j \boldsymbol{\nabla}_{\perp j}\psi = 0$ is used, based on the binary interaction structure of the electromagnetic interparticle potential ψ.[4] An equivalent derivation based on kinetic theory is given in the Appendix. The pair of Eqs. (6) and (8) can be combined into a single equation if one makes the further and critical hypothesis that the beam is transversely homogeneous and extends up to a maximum radial size $r_b(s)$, in addition to being centered at $\mathbf{r}_o$. This is equivalent to saying that inside the beam $n = N_b/\pi r_b^2$ and $\psi = -|\mathbf{r} - \mathbf{r}_o|^2 K/2r_b(s)^2$, which we take as the profile for our potential. If we make this hypothesis and subtract Eq. (8) from Eq. (6) we obtain

$$\mathbf{r}_\delta'' = -\kappa_z(s)\mathbf{r}_\delta + \frac{K}{r_b(s)^2}\mathbf{r}_\delta, \tag{9}$$

where the notation $\mathbf{r}_\delta \equiv \mathbf{r} - \mathbf{r}_o$ is introduced. A schematic of the assumed beam distribution and corresponding vectors is shown in Fig. 1.

Equation (9) is solved with known techniques of physics of beams.[2,4] Considering the x motion, let us write $x_\delta = A_{x_\delta} w(s)\sin[\int^s \zeta(s)ds + \zeta_0]$ and substitute this expression into Eq. (9) to obtain the pair of equations

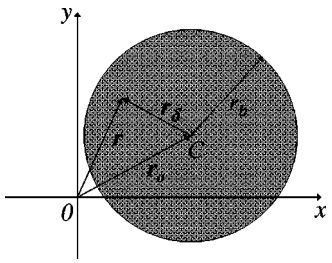

FIG. 1. Schematic of the beam distribution and corresponding vectors: C corresponds to the centroid position.

$$\zeta(s) = \frac{1}{w(s)^2},$$

$$\frac{d^2w(s)}{ds^2} + \kappa(s)w(s) = \frac{1}{w(s)^3}. \tag{10}$$

$\kappa(s) \equiv \kappa_z(s) - K/r_b(s)^2$ and A_{x_δ} is a constant of motion that can be expressed in the form

$$A_{x_\delta}^2 = \frac{x_\delta^2}{w^2} + \left(w\frac{dx_\delta}{ds} - \frac{dw}{ds}x_\delta \right)^2. \tag{11}$$

A similar calculation can be performed for the y motion, from which one forms the equilibrium distribution

$$f(\mathbf{r},\mathbf{r}',s) = (N_b/\pi^2\epsilon^2)\delta[\epsilon^{-1}(A_{x_\delta}^2 + A_{y_\delta}^2) - 1] \tag{12}$$

that automatically solves the Vlasov equation and generates the previously assumed constant density distribution, provided $w(s) = r_b(s)/\sqrt{\epsilon}$, which can be replaced into Eq. (10) to yield the envelope equation (1), written in its normalized form as

$$r_b'' = -\kappa_z(s)r_b + \frac{K}{r_b} + \frac{1}{r_b^3}, \tag{13}$$

if $s/S \to s, r_b/\sqrt{\epsilon S} \to r_b, \kappa_z S^2 \to \kappa_z$, and $SK/\epsilon \to K$; the rescaling does not alter the form of Eq. (8). We see indeed that as far as the focusing forces are linear, an equilibrium KV distribution can be formed for which the beam envelope obeys Eq. (1)—or its normalized form (13)—with constant emittance even when the centroid moves off-axis, $\mathbf{r}_o \neq 0$, following the dynamics dictated by Eq. (8). It is worth mentioning that these results can be generalized to a rigid-rotor equilibrium distribution[3] to describe an off-axis beam whose particles exhibit a rigid rotation around the centroid position with an arbitrary angular velocity. Note that the centroid motion and the envelope dynamics are uncoupled. In other words, centroid dynamics does not affect the known stability results for the envelope dynamics and is not affected by the latter as well. Stability analysis can be thus performed independently for envelope and centroid and our task is twofold: we wish to establish common regions of stability for both envelope and centroid, simultaneously determining whether previously found stable regions for the envelope dynamics are diminished by inclusion of centroid dynamics.

III. STABILITY ANALYSIS

A. Low-dimensional modeling

To accomplish our goal outlined in the preceding section we shall make use of the so-called Newton–Raphson stability algorithm in two instances: to locate periodic solutions of Eqs. (8) and (13), and to establish the stability boundaries for these periodic solutions. The code for stability boundaries actually makes use of the code finding periodic orbits as a subroutine. In the subroutine, orbits are characterized by their stability index α which lies on the interval $|\alpha| < 1$ if the orbit is stable. The main code then takes α as determined by some parameter p in the form $\alpha = F(p)$, which can be at least numerically obtained. For a given α one writes $p = \tilde{p} + \delta p$, where $\tilde{p}$ is a trial solution and δp is small. One finally obtains $\delta p \sim \Delta\alpha/(\partial F/\partial p)_{\tilde{p}}$ with $\Delta\alpha \equiv \alpha - F(\tilde{p})$ and refines the solution with $\tilde{p}_{new} = \tilde{p} + \delta p$. This is the essence of the algorithm and the boundaries will be determined when we set $\alpha = \pm 1$. We shall take p as the parameter measuring the intensity of the focusing magnetic field, $p \to \sigma_0$, and will search for stability regions in diagrams of the type σ_0 versus Δ. Although other parametric quantities can be used to represent the present setting,[14] ours appear to be more manageable in view of the various not so straightforward simulations maping stability boundaries in the presence of nonlinearities arising from perveance effects.

As mentioned in the Introduction, several regions of stability and instability for the envelope alone can be found as σ_0 changes. For sufficiently small values of the magnetic field one can always find stable orbits which become unstable when one crosses a period doubling threshold, diving into a region where $\alpha_{envelope} < -1$. The unstable region is cleared as the magnetic field continues to increase bringing the stability index back to $\alpha_{envelope} > -1$. As the field increases further, a mechanism called gap bifurcation destroys the matched solution at $\alpha_{envelope} = +1$ and recreates it at yet larger values;[9] the cycle is then repeated.[8]

As for the centroid motion, one can make some estimates when one realizes that the governing equation (8) is an equation of the Mathieu type. Since $\kappa_z(s)$ may be a complicated function due to the field profile we do not know in detail the behavior of Eq. (8), but given the general properties of Mathieu's equations, one can expect stable solutions while σ_0 remains sufficiently away from multiples of π; instability is therefore expected when one somehow approaches $\sigma_0 \sim n\pi$.

We presently extend the technique applied in a previous analysis performed on envelope stability alone,[7] and, as mentioned earlier, draw the stability boundaries $\alpha = \pm 1$ now simultaneously for both envelope and centroid equations in order to map the profusion of stable and unstable regions of the complete envelope-centroid system.

The corresponding distribution of unstable and stable regions is displayed in Fig. 2 where we take $\eta = 0.2$, with Δ ranging from $\Delta = 0.1$ to $\Delta = 10^4$. As pointed out, small values of Δ correspond to almost harmonic lattices, while large values associate to sharp-edged ones. What we see here can be phrased as follows. Given the complete independence be-

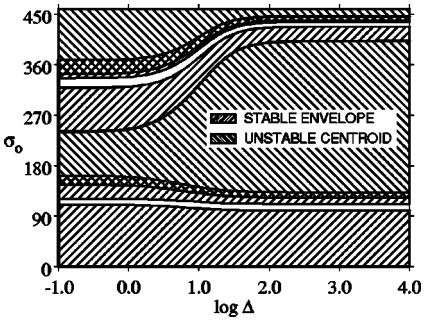

FIG. 2. Parametric diagram indicating stable envelope regions (slashed lines) and unstable centroid regions (backslashed lines) for $\eta=0.2$ and $K=5.0$.

tween envelope and centroid motion, stability regions of r_b remain as calculated previously.[7] Stable regions for the envelope dynamics are represented here by slashed lines, and *un*stable regions for the centroid are represented by backslashed lines—former stable regions for the envelope which have been destabilized by the centroid are thus represented by the crossing of these two types of line. The first region of stability for the envelope dynamics always bifurcates from the $\sigma_0=0$ axis for all lattice profiles and the centroid is always stable there. As the magnetic field grows, one first meets the period doubling region where the envelope becomes unstable (although still existent). For higher fields the envelope regains stability and it is within this region of restored envelope stability that the centroid becomes unstable for the first time. This is thus one critical region of our analysis where the envelope alone is still stable but the centroid, and the overall dynamics, no longer is; note that the destabilized regions occupies almost 50% of the previously stable region. While the centroid is unstable the mechanism we call gap bifurcation[9] destroys the matched envelope orbit and recreates it for larger fields, when the centroid has already retrieved its stable dynamics; we see that the gap bifurcations separate adjacent zones of existence for matched solutions. From this point on, the same kind of behavior repeats, with the unstable centroid dynamics occupying even more than 50% of the next previously stable region where it lays upon now. One can therefore conclude that the centroid dynamics becomes influential within parametric regions where the envelope alone would be in operational conditions, which is relevant information as one extends beam focusing schemes beyond the strong $\sigma_0=90°$ period doubling envelope instability. In any case, it may be appropriate to emphasize that entire stable regions of all zones remain untouched by centroid instabilities, namely, the regions immediately following gap bifurcations and prior to the direct period doubling sequences.

B. Full multiparticle simulations

We validate our low-dimensional findings with numerical simulations involving a large number $N_b=8000$ of macroparticle charged rods interacting via a pairwise electromagnetic interaction.[5] The choice $\sigma_0=155°, \Delta=10^{-1}$ places us right in a region where envelope is stable but centroid is not.

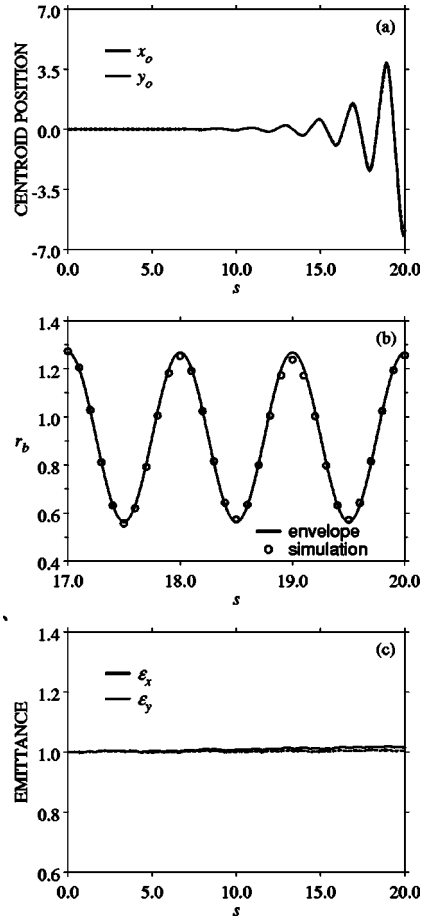

FIG. 3. Multiparticle simulations validating the low-dimensional results. $N_b=8000, \eta=0.2, \sigma_0=155°, \Delta=10^{-1}$, and $K=5.0$. (a) The centroid dynamics, (b) comparison of the envelope equation (13) and multiparticle simulations, and (c) emittance as obtained by the multiparticle simulations.

Accordingly, as we start from very small values of $|\mathbf{r}_o|$ and $|\mathbf{r}_o'|$, Fig. 3(a) reveals that the centroid motion develops the typical exponential growth of unstable dynamics and Fig. 3(b) shows that all the while the envelope is very precisely described by the stable dynamics that results from Eq. (13). Also, Fig. 3(c) indicates that emittance is well conserved as time evolves, an indicative that the envelope dynamics operates as expected. Emittance is evaluated from

$$\epsilon_\chi = 4[\langle\chi^2\rangle\langle\chi'^2\rangle - \langle\chi\chi'\rangle^2]^{1/2}, \quad \chi = x - x_0, y - y_0 \tag{14}$$

and the envelope from

$$r_b = [2\langle(x-x_o)^2 + (y-y_o)^2\rangle]^{1/2} \tag{15}$$

the brackets indicating average over macroparticles. In general one concludes that the dynamics indeed decouples into a stable envelope dynamics and an unstable centroid dynamics.

IV. INFLUENCE OF CONDUCTING PIPES

We now investigate the influence of a cylindrical conducting pipe encapsulating the beam. Conducting pipes isolate the beam and exert action over beam transport due to the buildup of induced charges over its surface. We know that the influence on the pure envelope dynamics is in general

small;[13] in cases with solenoidal geometry like ours it is virtually null. On the other hand, the influence of pipes on the centroid dynamics was analyzed in smooth regimes where the lattice is approximately described as an average continuous entity.[6] In this regular case it has been shown that the pipes introduce a nonlinear effect capable of destabilizing the centroid equilibrium only for a relatively restricted range of small values of σ_0. We are willing to go beyond the smooth-beam approximation and see what happens when the lattice periodicity is fully preserved in the model. We actually expect to see some degree of nonintegrable dynamics, since our system becomes a nonlinear one with one and a half degree of freedom. The central issue is to find out whether or not the presence of nonintegrable trajectories can affect substantially the corresponding phase space.

In the absence of conducting pipes the governing equation for the centroid is simply the linear equation (8). When the pipe is present, the induced charge over its surface can be represented as an image charge placed beyond the cylindrical walls. Assume again that the beam is a thin filament located along the x axis. The technique of image charges then allows us to conclude that its image is located at $x_{image}(s)=a^2/x(s)$, where a is the pipe radius, and charged with the opposite charge of the beam itself.[12] This concludes the construction of the image. The potential of a cylindrical rod placed at x_o is proportional to $\ln(x-x_o)$, from which one finally obtains the force acting on the beam due to its image as $+Kx/(a^2-x^2)$ where we recall that K is the perveance. The governing equation for the centroid is therefore augmented into the following form:

$$x_o'' = -\kappa_z(s)x_o + \frac{Kx_o}{a^2 - x_o^2}. \tag{16}$$

We analyze Eq. (16) numerically via Poincaré plots and for simplicity omit the qualitatively similar y_o dynamics. In Fig. 4(a) we display a typical phase plot for the beam centroid x_o' versus x_o at $\Delta=0.1$ and $\sigma_0=140°$, with the pipe radius a chosen as approximately five times larger than the corresponding maximum $r_b, a/(r_b)_{max}\approx 5.0$, so as to represent the usual condition of pipes reasonably larger the encapsulated beams. What we observe is that although the very central region $x_o\to 0$ is free of chaotic orbits, its surroundings are already heavily occupied by the presence of nonintegrable orbits which extends up to the walls. For comparison we also display situations where approximations are made: walls are removed in panel (b), and the smooth-beam approximation $\kappa_z=$const is used in panel (c). In both cases of panels (b) and (c) the dynamics becomes regular, so we may have a good notion about the relevant role of chaotic motion in the system. The conclusion is clear: one must be careful to place the beam aligned and close to the central axis, for otherwise particles can be swept away due to chaotic diffusion. Of course, even with the beam located near the axis, one still has to observe the criteria analyzed in previous sections to secure stability.

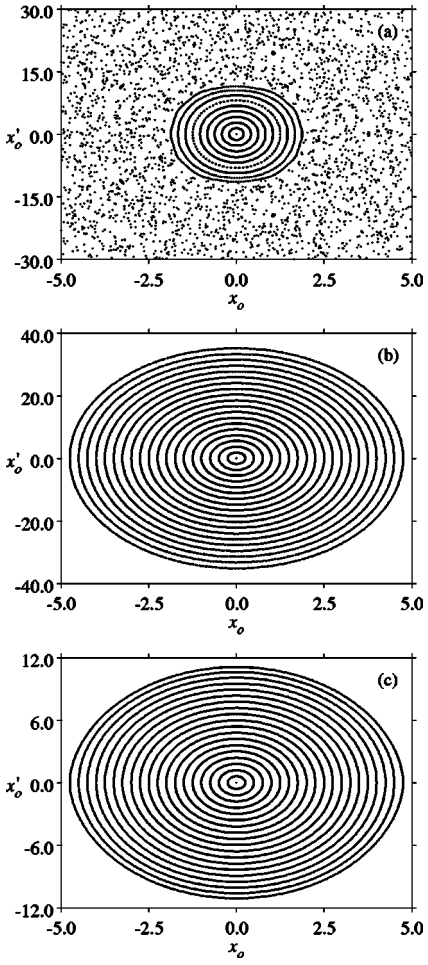

FIG. 4. Poincaré plots of x_o' versus x_o as obtained from Eq. (16). In (a), $\eta=0.2$, $\sigma_0=140°$, $\Delta=10^{-1}$, $K=5.0$, and $a=5.0$. In (b), the pipe is removed ($a\to\infty$) and, in (c), the smooth-beam approximation $\kappa_z=$const. is used. The other parameters are the same as in (a).

V. FINAL REMARKS

We have investigated the role of centroid dynamics in the stability of charged beams transported along periodical focusing channels.

Analysis has been directed to KV beams for which we show that the centroid and envelope dynamics become exactly uncoupled if focusing forces are linear in the coordinates. As the focusing intensity and profile are varied, we show that unstable centroid regions in the appropriate parameter space can partially overlap with stable envelope regions. This indicates that overall stable regions are certainly smaller than the ones described in the previous analysis of envelope dynamics alone.[7]

As our results indicate, unstable centroid dynamics develops in parametric regions where the pure envelope dynamics retrieves its stable motion after period doublings direct and inverse sequences. Previous analysis of the pure envelope dynamics already point to the fact that in these regions the envelope can be unstable against symmetry breaking quadrupolelike perturbations, not included in the axisymmetric approach used here.[15] Full multiparticle simulations show that small emittance growth may also be present in these very same regions.[5] Emittance growth is very small

and quadrupolelike perturbations are confined to relatively narrow regions, so these instabilities are not of immediate concern if one is willing to operate there. However, centroid dynamics occupies substantially large fractions of these regions, from which we conclude that care should be taken to avoid the centroid instabilities mostly. All low-dimensional results based on envelope and centroid equations are fully corroborated by multiparticle simulations.

Inclusion of image charge effects due to the presence of conducting walls of pipes enclosing the beam is also considered. It is shown that although image charges do not affect centroid stability at the central equilibrium, large chaotic activity is generated in its vicinity due to the nonlinear terms associated with the image electromagnetic potential. Chaotic activity is not present in smooth-beam approximations and arises from the nonlinear beating of the lattice periodicity with the natural frequency of the centroid oscillations. The conclusion on this latter issue is that in order to avoid diffusion due to nonintegrable effects, beams must be injected with sufficient proximity to the axial region.

ACKNOWLEDGMENT

This work was partially supported by CNPq, Brazil.

APPENDIX: DERIVATION OF CENTROID DYNAMICS BASED ON KINETIC THEORY

Consider the Vlasov–Maxwell system governing a two-dimensional distribution function $f=f(\mathbf{r},\mathbf{r}'\equiv\mathbf{v},s)$:

$$\frac{\partial f}{\partial s}+\mathbf{v}\cdot\boldsymbol{\nabla} f+(-\kappa_z\mathbf{r}-\boldsymbol{\nabla}\psi)\cdot\boldsymbol{\nabla}_{\mathbf{v}}f=0, \tag{A1}$$

$$\nabla^2\psi=-2\pi K/N_b n(\mathbf{r},s), \tag{A2}$$

$$n=\int f\,d\mathbf{v}. \tag{A3}$$

If one multiplies Eq. (A1) by $\mathbf{r}$ and integrates over phase space one gets

$$\overline{\mathbf{r}}'=\overline{\mathbf{v}}, \tag{A4}$$

where $(\overline{\mathbf{r}},\overline{\mathbf{v}})\equiv N_b^{-1}\int(\mathbf{r},\mathbf{v})f\,d\mathbf{r}\,d\mathbf{v}$, with the normalizing integral $N_b\equiv\int f\,d\mathbf{r}\,d\mathbf{v}$. In addition to that, if one now multiplies the same Eq. (A1) by $\mathbf{v}$ and integrates over phase space, one has

$$\overline{\mathbf{v}}'=-\kappa_z\overline{\mathbf{r}}-\overline{\boldsymbol{\nabla}\psi}, \tag{A5}$$

where $\overline{\boldsymbol{\nabla}\psi}\equiv N_b^{-1}\int\nabla\psi f\,d\mathbf{r}\,d\mathbf{v}$ is obtained by integration by parts of the $\boldsymbol{\nabla}_{\mathbf{v}}$—term in velocity space. Note that Eq. (A5) has the same statistical origins as Eq. (8) of the main text so what remains to be shown is that $\overline{\boldsymbol{\nabla}\psi}=0$ on kinetic grounds. To this end we first use Eq. (A3) to write

$$\overline{\boldsymbol{\nabla}\psi}=N_b^{-1}\int\boldsymbol{\nabla}\psi f\,d\mathbf{r}\,d\mathbf{v}$$

$$=N_b^{-1}[-N_b/(2\pi K)]\int\boldsymbol{\nabla}\psi\nabla^2\psi\,d\mathbf{r}. \tag{A6}$$

Then we note that the integrand of the last integral of Eq. (A6) can be cast into the more appropriate form

$$\boldsymbol{\nabla}\psi\nabla^2\psi=\boldsymbol{\nabla}\cdot[\boldsymbol{\nabla}\psi\boldsymbol{\nabla}\psi-\mathbf{I}(\boldsymbol{\nabla}\psi)^2/2], \tag{A7}$$

where the unit dyadic $\mathbf{I}$ reads $\mathbf{I}\equiv\hat{\mathbf{x}}\hat{\mathbf{x}}+\hat{\mathbf{y}}\hat{\mathbf{y}}$, where $\hat{\mathbf{x}}$ and $\hat{\mathbf{y}}$ are the versors along x and y. Finally, given that $\boldsymbol{\nabla}\psi\to 0$ as $x^2+y^2\to\infty$ for beams in free space, Gauss theorem then shows that $\overline{\nabla\psi}=0$, so $\overline{\mathbf{v}}'=-\kappa_z\overline{\mathbf{r}}$.

For bounded but nearly symmetric beams, $\boldsymbol{\nabla}\psi=\pm\hat{\mathbf{n}}|\boldsymbol{\nabla}\psi|$ at the pipe walls, where $\hat{\mathbf{n}}$ is the unit vector normal to the wall, and the surface integral still vanishes since $|\boldsymbol{\nabla}\psi|$ is approximately constant there. This is useful information in bounded systems when the beam is not yet excessively displaced from the central axis.

The centroid therefore obeys an equation of the form

$$\overline{\mathbf{r}}''=-\kappa_z\overline{\mathbf{r}} \tag{A8}$$

if f obeys the Vlasov equation.

What we do next is to construct the beam centered at $\overline{\mathbf{r}}$ [which we denote by $\mathbf{r}_o(s)$ in the text], i.e., around the centroid, to show that the quantities A_{x_δ} and A_{y_δ} are conserved quantities with which one can form the argument of the KV-like distribution. The KV-like distribution defined this way consequently solves the Vlasov equation precisely because it depends on conserved quantities. Finally we reach the consistency condition $w=r_b/\sqrt{\epsilon}$ by demanding that the density drops to zero beyond r_b and is flat otherwise. We finally point out that for the KV-like distribution of the present paper, defined by Eq. (12) and depending on function $\mathbf{r}_o(s)$, it is easily seen that if one calculates averaged coordinates and velocities one obtains

$$\overline{\mathbf{r}}\equiv N_b^{-1}\int\mathbf{r}f_{\mathrm{KV}}d\mathbf{r}\,d\mathbf{v}=\mathbf{r}_o(s), \tag{A9}$$

$$\overline{\mathbf{v}}\equiv N_b^{-1}\int\mathbf{v}f_{\mathrm{KV}}d\mathbf{r}\,d\mathbf{v}=\mathbf{r}_o'(s). \tag{A10}$$

One concludes that if f_{KV} is a solution of the Vlasov–Maxwell set, $\mathbf{r}_o$ must obey an equation like Eq. (A5) as we impose in the text from the start. There is nothing prohibiting the centroid to move, provided Eq. (A8) be satisfied.

[1] C. Chen and R. C. Davidson, Phys. Rev. Lett. **72**, 2195 (1994).
[2] C. Chen and R. C. Davidson, Phys. Rev. E **49**, 5679 (1994).
[3] C. Chen, R. Pakter, and R. C. Davidson, Phys. Rev. Lett. **79**, 225 (1997).
[4] R. C. Davidson and H. Qin, *Physics of Intense Charged Particle Beams in High Energy Accelerators* (World Scientific, Singapore, 2001).
[5] R. Pakter and F. B. Rizzato, Phys. Rev. E **65**, 056503 (2002).
[6] M. Hess and C. Chen, Phys. Plasmas **7**, 5206 (2000).
[7] J. S. Moraes, F. B. Rizzato, and R. Pakter, Phys. Plasmas **10**, 4811 (2003).
[8] R. Pakter and F. B. Rizzato, Phys. Rev. Lett. **87**, 044801 (2001).
[9] F. B. Rizzato and R. Pakter, Phys. Rev. Lett. **89**, 184102 (2002).
[10] C. J. Struckmeier and M. Reiser, Part. Accel. **14**, 227, (1984); see also P. M. Lapostolle, IEEE Trans. Nucl. Sci. **NS-18**, 1101 (1971); F. J. Sacherer, *ibid.* **NS-18**, 1105 (1971); I. Hofmann, L. J. Laslett, L. Smith, and I.

Haber, Part. Accel. **13**, 145 (1983).
[11]I. M. Kapchinskij and V. V. Vladimirskij, *Proceedings of the International Conference on High Energy Accelerators*, edited by L. Kowarski (CERN, Geneva, 1959), p. 274.
[12]J. D. Jackson, *Classical Electrodynamics* (Wiley, New York, 1975).
[13]B. L. Qian, J. Zhou, and C. Chen, Phys. Rev. ST Accel. Beams **6**, 014201 (2003).
[14]S. M. Lund and B. Bukh, Phys. Rev. ST Accel. Beams **7**, 024801 (2004).
[15]J. S. Moraes, R. Pakter, F. B. Rizzato, and C. Chen, Phys. Scr., T, **T 107**, 145 (2004).